

Simulation of Deformation Behavior of Porous Titanium Using Modified Gurson Yield Function

E. Ansari Basir and K. Narooei*

Department of Materials Science and Engineering, K. N. Toosi university of Technology

Abstract: In this research, the stress-strain curve of porous Titanium, as a common material for biomedical application, was predicted using the mechanical properties of fully solid Titanium experimental data. Modified Gurson model (Gurson-Tvergaard-Needleman (GTN) model) was used to predict the plastic response of porous Titanium in compaction. Different values of GTN parameters were used for different initial porosity. It was recognized that volume constancy assumption during plastic deformation of porous media cannot be satisfied due to both of changes in porosity and hydrostatic stress contribution on yielding. It was found that consideration of porosity variation is necessary during deformation for accurate modeling. Also, porous samples represented the same lateral expansion under less axial displacement relative to fully solid sample regarding the GTN model. The stress distribution of porous samples was different from solid sample considering the GTN model and this was predicted different shear banding. Evolution of porosity during deformation leads to linear like stress response in the plastic deformation regime.

Keywords: Modified Gurson model (GTN), Porous Titanium, Finite element method, Plastic deformation, Compaction

1. Introduction

In recent years, metallic materials have been used in artificial organic parts. Gibson and Ryan et al presented advantages of metallic implants due to their high strength and well toughness in comparison with polymeric, ceramic, and glass based materials [1, 2]. Dynamic deformation of metal foils using micro-blast waves for medical application was investigated by Nagaraja et al [3]. Materials for biomedical utilization must have appropriate compatibility with the living media. For example, human body as a corrosive environment can destruct corrosion sensitive materials. Moreover, mechanical characteristics have a critical effect on the efficiency of biomaterials.

Mechanical mismatch between organic and artificial manufactured parts of body can lead to failure of biomedical parts. It is known that the efficiency of some replaced organic parts such as dental implants depends on the stress distribution of the surrounding bone [4]. Stress shielding is a known result of difference between stiffness of organs and implants. In past, compatible coats with stiffness like to bone were used to bypass difficulties of mismatch between bone and implant [5, 6] however, coating alone could not solve such problems. Another way to solve the problem of mismatch between bone and implant is the presence of porosity in the structure of materials. In fact, materials with high levels of strength can be matched with mechanical properties of organic parts by means of porosity control. Facilitation of cells proliferation, promotion of vascularization, and making compatibility between different parts have been investigated taking into account porous implants [7].

Identifying the mechanical properties of porous materials is necessary to simulate the deformation of these materials. Sintered iron powder was investigated by Schneider and Yuan under fatigue test with

different material porosities [8]. It was found that a model contains nonlinear kinematic and isotropic hardenings can take into account the effect of cyclic loading on the material fracture [8]. Kovacik investigated the correlation between Young's modulus and porosity in sintered iron, porous alumina, sintered glass and Titanium alumide [9]. Upper-bound approach was introduced by Tirosh and Iddan to estimate the required load for the forming of porous materials [10]. They found the porosity can affect the forming load depending on the hydrostatic stress.

A well-known material, which is widely used for biomedical applications, is porous Titanium. Some research pointed out that porous Titanium can be used as biomaterial because of good corrosion resistance, high strength, and low density [11, 12]. Open pores Titanium was investigated by Imwinkelried and it was shown that foams have stiffness and yield strength between cancellous and cortical bone [13]. Deformation behavior of intermediate porosity interconnected Titanium foams was studied by Singh et al [14]. Porous Titanium foams contain macro pores formed by the space holder and the micro pores formed by incomplete sinter were modeled by Wenjuan et al [15]. The micro scale model confirmed the experimental data.

Finite element as a strong method to anticipate the behavior of porous materials is widely used in recent years. The effect of diameter variation of cellular lattice structures on elastic modulus was investigated by Ravari et al using beam and solid elements [16]. Sinter powder compaction under different frictional condition during forging process was studied by Huang and Cheng [17]. Effect of hydrostatic pressure on the densification of porous iron containing 0.3-11% porosity was studied by Biner and Spitzig [18]. Some of these works used Gurson model to simulate compression of different porous materials.

Gurson model has been widely used to predict the plastic deformation of porous materials due to contribution of porosity as a parameter of yield function. In fact, Gurson model can be seen as a modification of von Mises criterion, which consider the effect of porosity in the body. Therefore, this model can be used conveniently for numerical studies. Tvergaard and Needleman modified the Gurson model by adding some parameters for better correlation with experimental studies and called the new criterion GTN [19, 20]. Becker et al recommended more precise values for these parameters [21]. Abbasi et al represented an inverse procedure to estimate material parameters of the GTN model based on the plastic damage of steel [22]. Spitzig et al investigated relation of porosity density and growth of voids during compaction of iron to provide a more general form of the Gurson model [23].

In this research, the GTN model was used to relate mechanical properties of fully solid to porous Titanium. To this end, two non-linear problems were solved using Newton-Raphson method. Some Titanium samples with different porosity were considered as test samples. Different values of GTN model parameters were adopted to achieve appropriate correlation with experimental data. Porosity reduction during compaction was investigated by numerical solution to satisfy change of material density during compaction.

2. GURSON Model and Plasticity Theory

Many yield functions for porous materials have been suggested in recent years. The Gurson model has been widely used to predict the plastic deformation of porous materials. Here, the modified Gurson model was considered for the yielding of the porous Titanium as [18]:

$$\phi = \left(\frac{\bar{\sigma}}{\sigma_M} \right)^2 + 2fq_1 \cosh\left(\frac{3}{2}q_2 \frac{tr(\sigma)}{\sigma_M} \right) - 1 - q_3 f^2 \quad (1)$$

where, $\bar{\sigma}$ is the effective stress, σ_M the flow stress of dense Titanium matrix and f the volume fraction of porosity such that $0 \leq f \leq 1$. It is worth mentioning that in the special case of fully solid sample

($f = 0$), Eq. 1 is reduced to the well-known von Mises yield criterion. The coefficients q_1 , q_2 , and q_3 have been determined by Tvergaard and Needleman to achieve better correlation with experimental studies such that $q_1 = 1.5$, $q_2 = 1.0$ and $q_3 = q_1^2$ [19, 20].

The general shape of yield equation for porous materials can be written as:

$$\phi = \phi(\sigma, \alpha, f) \quad (2)$$

Here, the parameter α represents the hardening parameter (isotropic or kinematic hardening). In this paper, only the isotropic hardening is considered and thereby α is a scalar value parameter.

In comparison with Eq. 1 and because α shows the evolution of yield surface, it can be written:

$$\sigma_M = \sigma_{M0} + K(\alpha) \quad (3)$$

where, σ_{M0} is considered as the initial flow stress of metal matrix and $K(\alpha)$ represents the hardening behavior. The current yield strength can be calculated from the previous yield strength as [24]:

$$(\sigma_M)_{n+1} = (\sigma_M)_n + \Delta K_{n+1} \quad (4)$$

The non-linear hardening that was considered in this research has been presented in Fig. 1. For modeling of non-linear hardening 30 points of Fig. 1 were extracted and the slope between each of two points was calculated. The hardening between each of two points was considered to be linear leads to totally non-linear hardening model.

Assuming associated flow rule leads to the evolution of the increment of plastic strain as follow:

$$d\varepsilon_{ij}^p = \gamma \frac{\partial \phi}{\partial \sigma_{ij}} \quad (5)$$

Here $d\varepsilon_{ij}^p$ represents the increment of plastic strain of porous body and γ denotes the consistency parameter. Total plastic strain can be stated as:

$$(\varepsilon_{ij})_{n+1}^p = (\varepsilon_{ij})_n^p + \Delta\gamma \frac{\partial \phi}{\partial \sigma_{ij}} \quad (6)$$

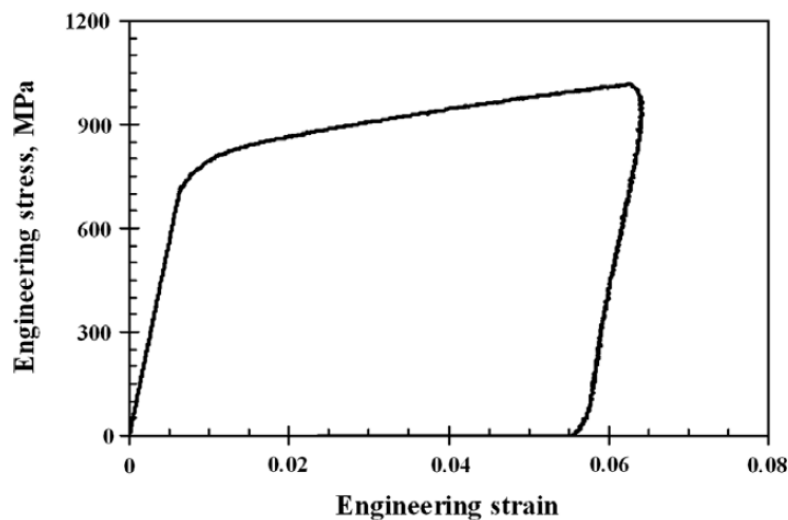


Fig. 1. Stress-Strain curve of fully solid Titanium in compression [14].

Due to the presence of porosity it is necessary to determine the relation of total observed plastic deformation and plastic strain of metal matrix. Plastic strain of the matrix $d\varepsilon_M^p$ is assumed to vary according to equivalent plastic work as [18]:

$$(1-f)\sigma_M d\varepsilon_M^p = \sigma_{ij} d\varepsilon_{ij}^p \quad (7)$$

Evolution of porosity is another important parameter during of loading. The porosity evolutions can be taken into account in three main phases including nucleation, growth and coalescence [17, 22]. For simplicity, in this paper just growth of porosity is assumed as [18]:

$$(df)_{n+1} = (1-f_n)(d\varepsilon_{11}^p + d\varepsilon_{22}^p + d\varepsilon_{33}^p)_{n+1} \quad (8)$$

Total porosity fraction can be obtained as:

$$f_{n+1} = f_n + (df)_{n+1} \quad (9)$$

So, according to Eq. 9 the porosity during deformation is changed. Regarding above brief discussion on the GTN formulation, in the next section the mechanical properties of porous Titanium are presented.

3. Porous Titanium Mechanical Properties

To simulate the deformation of porous materials, six Titanium samples with different percentage of porosity were compressed. The elastic modulus of porous samples were calculated by means of power law relationship as [9, 11]:

$$E = E_0 \left(1 - \frac{f}{f_c}\right)^n \quad (10)$$

where, E_0 is the Young modulus of fully solid material and f_c is the porosity at which the effective Young modulus (E) becomes zero. As it has been stated by Nakajima, the f_c can be considered as $f_c = 1$ [11]. The percentage of porosity, appropriate values of n in Eq. 12, and calculated effective Young modulus for different samples were presented in Table 1. First sample was assumed to be fully solid (0% porosity) and the second and last samples were chosen for comparison with Singh et al research [14]. Remaining samples were chosen for comparison with Imwinkelried research where it was assumed the non-porous material properties are as the first row of Table 1 [13].

The initial yield strength of the fully solid Titanium was assumed as 650 MPa [13]. The stress-strain curve of fully solid Titanium during compression was shown in Fig.1. This curve was used to evaluate the behavior of metal matrix during plastic deformation. The stress-strain curves of different porous Titanium samples during compression can be seen in Fig. 2 [13, 14]. Relation of Figs. 1 and 2 can be recognized using FE method.

Table 1. Young modulus and fitting parameter of different porous Titanium samples.

sample	Porosity (%)	E (GPa)	n	Poisson Coefficient (ν)
1	0	112.3	-	0.317
2	50.6	8.0	3.74	0.307
3	57.7	5.5	3.5	0.317
4	59.9	5.0	3.4	
5	62.5	4.0	3.4	
6	63.9	2.0	3.95	0.365

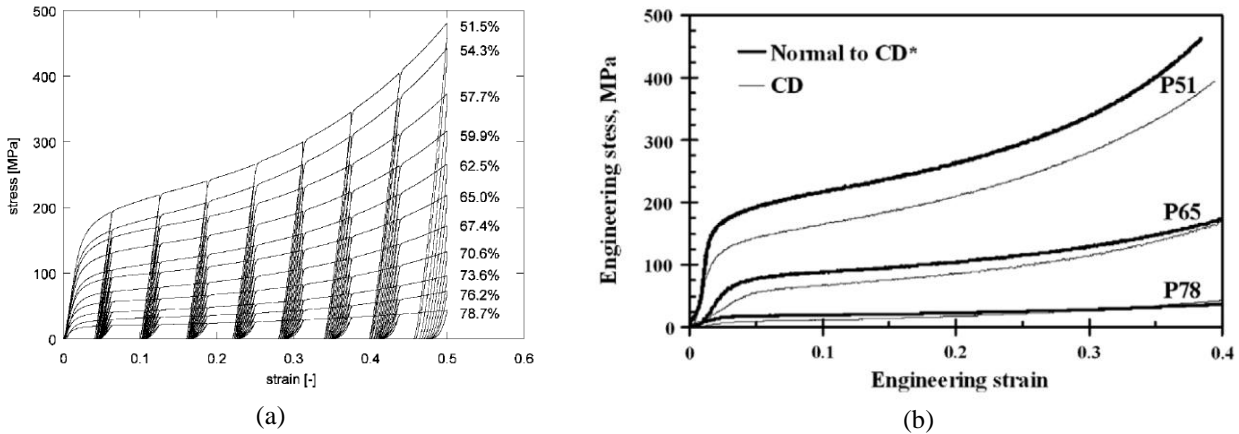


Fig. 2. Stress-strain curves for Titanium with different levels of porosity during compaction: (a) Imwinkelried [13] and (b) R. Singh et al [14].

4. FEM Procedure

A $16 \times 16 \text{ mm}^2$ sample for FEM simulation was considered. Here, due to symmetry only $8 \times 8 \text{ mm}^2$ of sample was meshed with 225 quadrilateral elements. This assumption leads to reduction of computational time in addition to increase of numerical stability due to avoiding rigid body motion. Fig. 3 shows the geometry and boundary conditions for the compression test. Three sets of boundaries were considered as follow. The top boundary was constrained in the X direction and applied prescribed displacement equal to 1.5 mm in the negative Y direction for porous samples and 1 mm for fully solid one. Left face was considered to be constrained in the X direction and bottom face was constrained in the Y direction as a result of symmetry. It should be noted in the contour plots, the full sample is presented by mirroring with respect to X and Y axes. Because of mesh distortion in top-right corner of body in the Lagrangian mesh, region A and B have been chosen for calculation of maximum and minimum stress and strains. The material and geometrical non-linearity were considered for the FE simulation of compaction in a written code [24, 25].

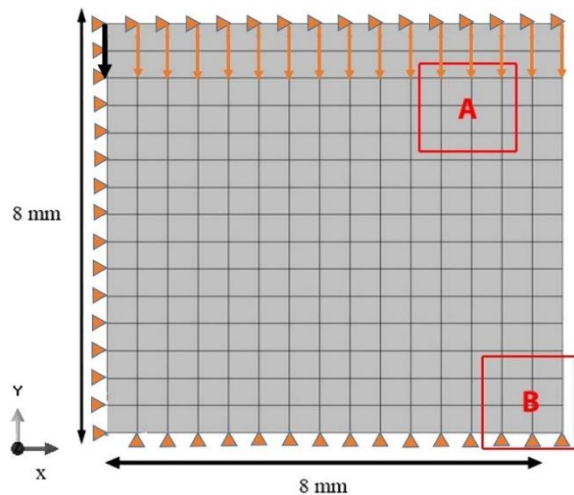


Fig. 3. Geometry and boundary condition of samples in FE simulation.

5. Results and Discussion

The main goal of this paper is to use the mechanical properties of fully solid material to predict the plastic behavior of porous samples. The predicted stress-strain curves of fully solid sample (sample 1) and its comparison with experimental one were shown in Fig. 5a. The stress-strain curve of sample 2 were shown

in Fig. 5b. Comparing of Figs. 5a and 5b reveals reduction of yield strength from 650 MPa to 120 MPa due to porosity, which is resulted from the effect of porosity in yield criterion (Eq. 1).

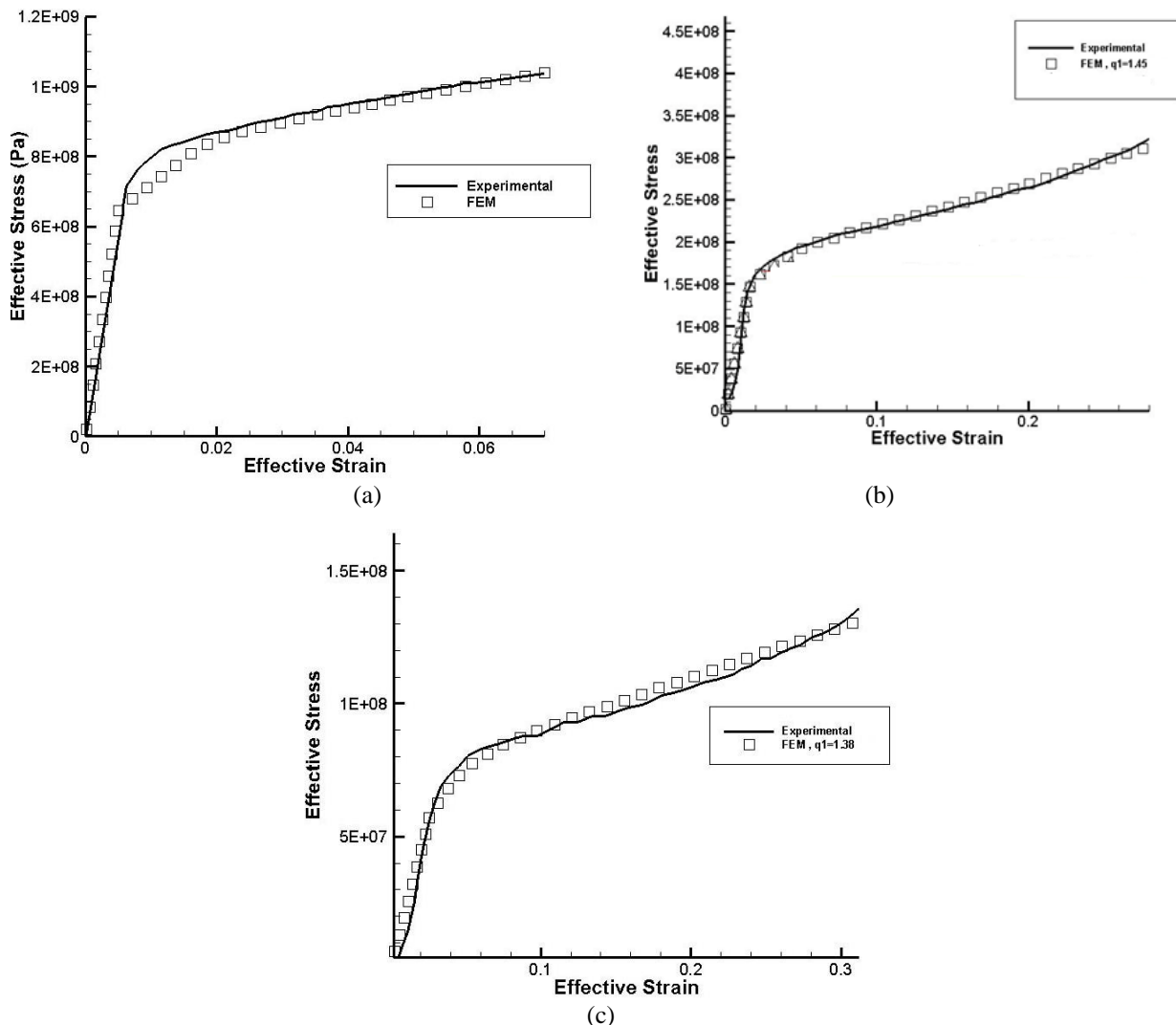


Fig. 5. Experimental [14] and numerical stress-strain curves of of compression: (a) sample 1 (0% porosity), (b) sample 2 (50.6% porosity), and (c) sample 6 (63.9% porosity).

As the initial yield strength of samples can be affected by many physical sources, the effect of them can be taken into account by adjusting parameters q_1 , q_2 , and q_3 in GTN model. Fitting of FE stress-strain curves to experimental curves by changing the value of q_1 and therefore, $q_3 = q_1^2$ is considered here. Changes of these parameters from what reporting by Tvergaard and Needleman [19, 20] was led to appropriate fitness of FE results to experimental data. The best fit of FE curves to experimental results was occurred by choosing $q_1 = 1.45$ for sample 2 as shown in Fig. 5b. Different simulated curves due to the change of q_1 for sample 3 (57.7% porosity) can be observed in Fig. 6a. As it can be observed, the best choice for this parameter in GTN model of sample 3 is $q_1 = 1.38$. The best fit to experimental FEM curves for samples 4-6 was also, reached by choosing $q_1 = 1.38$ as shown in Figs. 6b, 6c and 5c respectively. It is worth to mention that linear like plastic behavior of FE curves was resulted from the assumption of porosity evolution according to Eq. (10) [18].

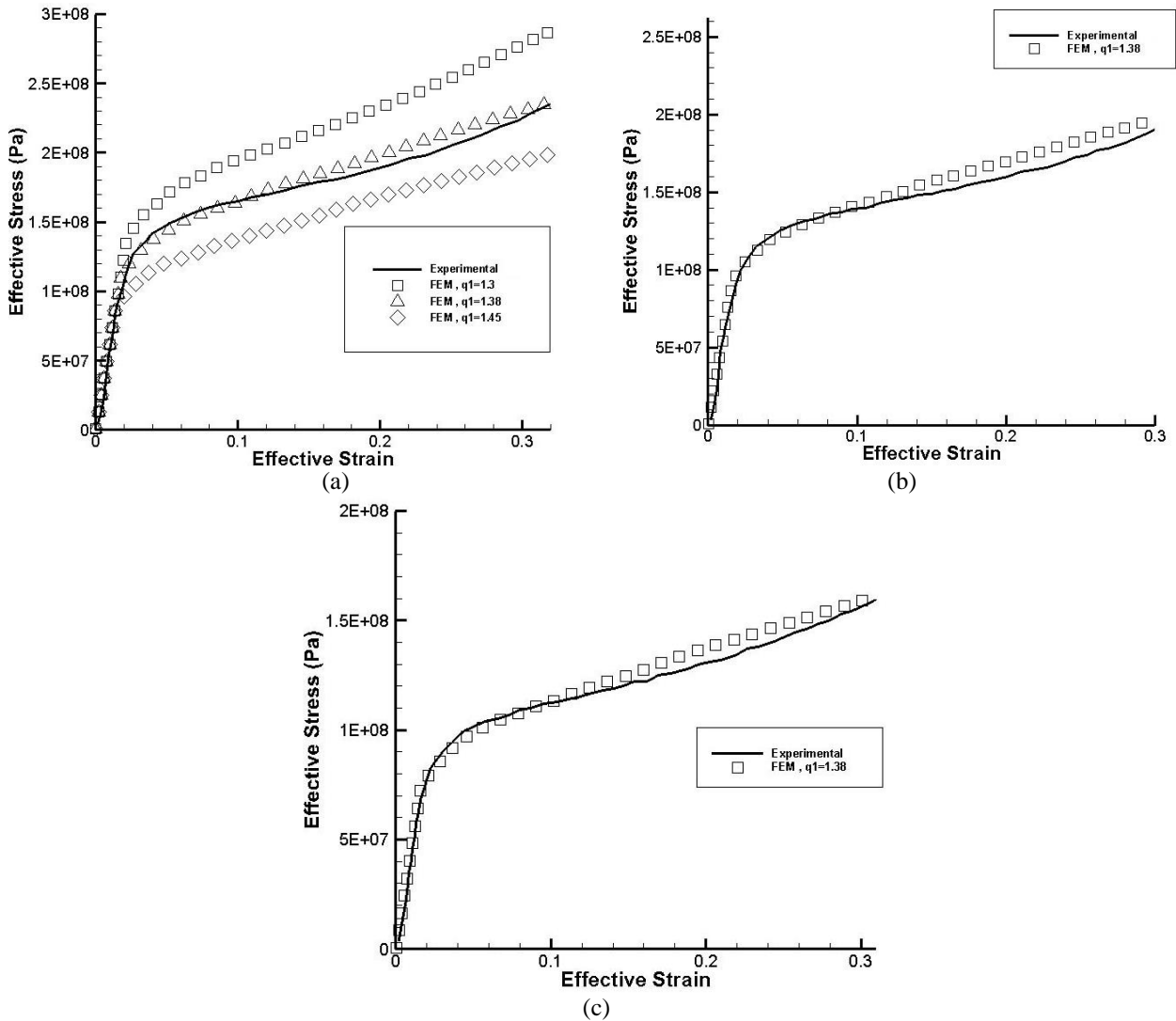


Fig. 6. Experimental [13] and different numerical stress-strain curves in compression of: (a) sample 3 (57.7% porosity), (b) sample 4 (59.9% porosity), (c) sample 5 (62.5% porosity).

Because of the dependency of yield criterion to trace of stress tensor, it can be concluded that the volume constancy cannot be satisfied in porous materials. This result is completely in agreement to the change of porosity and bulk compaction during deformation.

Investigation of stain, stress, and porosity distribution in deformed specimens leads to better insight for engineers in design. Regarding this, the stress and strain distribution in the deformed geometry can be observed in Figs.7 and 8 for different samples.

Comparing of Figs. 7a and b demonstrates that although the axial displacement of sample 1 is less than the porous samples (2 mm for sample 1 and 3 mm for porous samples), the lateral expansion of fully solid sample is equal to porous samples (1.8 mm in mid plane). This means more relative lateral expansion of fully solid sample. Furthermore, assessment of Figs. 7a and b indicates less maximum strain in fully solid sample due to less axial displacement.

The strain level in the corners of samples is local and not reliable due to mesh distortion. As mentioned before, the region A has been chosen near to the corners to investigate the maximum strain and stress values (Fig. 3). Reduction of maximum strain in region A due to increase of porosity can be seen in different parts of Fig. 7. This means that despite the same reduction of height of porous samples, the strain in different samples cannot be equal. This is because of the role of porosity in stress and strain distribution during compaction. Stress contours of different samples during compression were shown in Fig. 8.

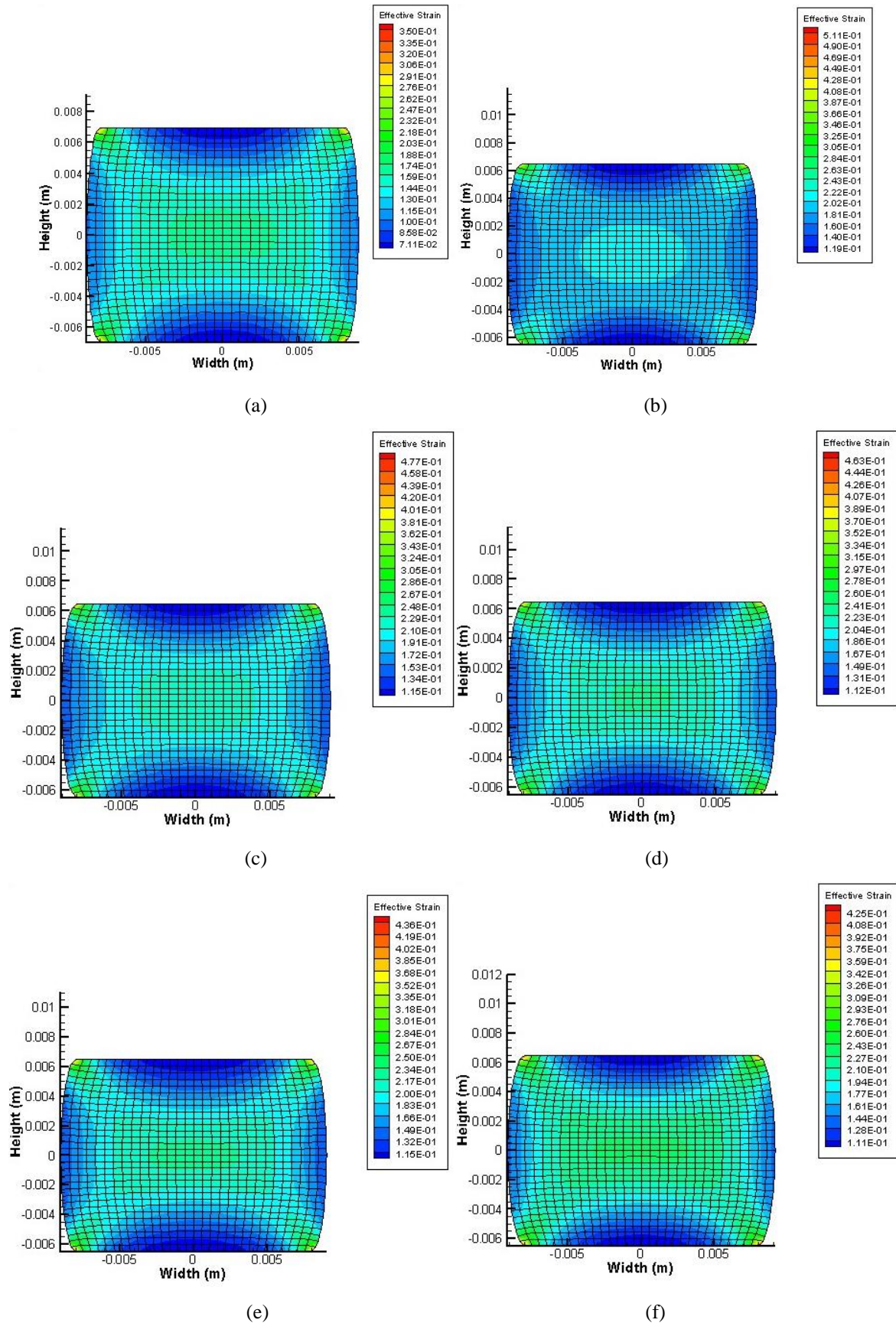


Fig. 7. Contour of effective strain of: (a) Sample 1, (b) Sample 2, (c) Sample 3, (d) Sample 4, (e) Sample 5, and (f) Sample 6.

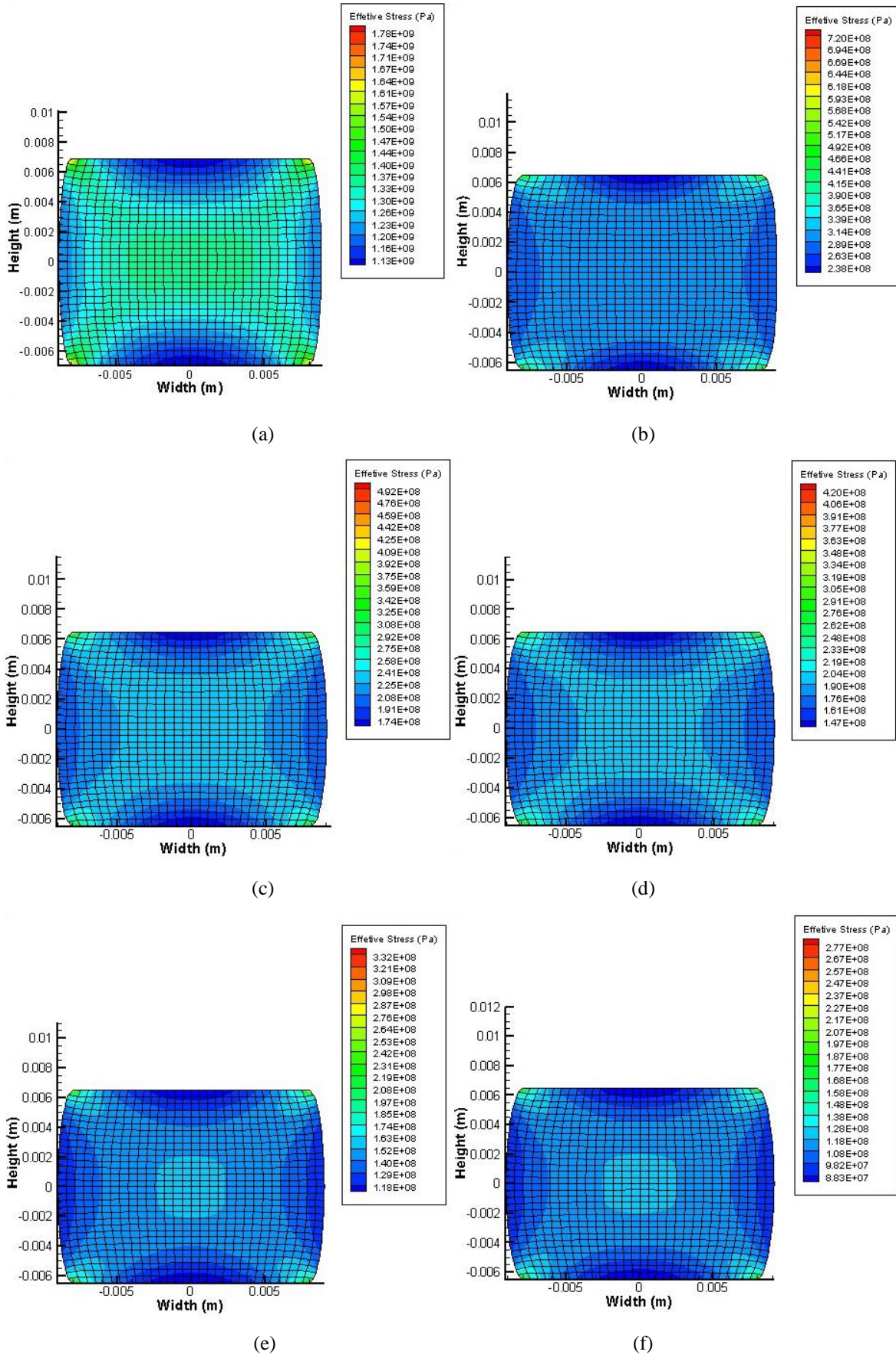


Fig. 8. Contour of effective stress of: (a) Sample 1, (b) Sample 2, (c) Sample 3, (d) Sample 4, (e) Sample 5, (f) Sample 6.

For sample 2 with 50.6% porosity (Fig. 8b) the maximum stress in region A has been reached about 500 MPa. In comparison with maximum stress of fully solid sample (1.5 GPa), an intensive drop in stress level can be observed. Also, the stress distribution in sample 2 is different from fully solid sample which is resulted of using different yield criteria. This means that presence of porosity has a critical role in stress levels and distributions of porous samples and in the stress analysis of these samples a suitable yield function should be considered. Comparing of stress contours of porous samples in Fig. 8 specified that the increase of porosity leads to the decreases of stress in samples as the increase of porosity affects the contribution of matrix plastic deformation. Inspection of stress distribution of samples in Fig. 8 indicates that the shear banding also affected by the porosity contribution. It is worth to mention, the porosity contribution was considered via the GTN model, and it indicates the necessity of selection of suitable yield function.

The porosity volume fraction distribution of different samples can be seen in Fig. 9. The maximum and minimum porosity of samples in these figures are occurred in regions A and B, respectively.

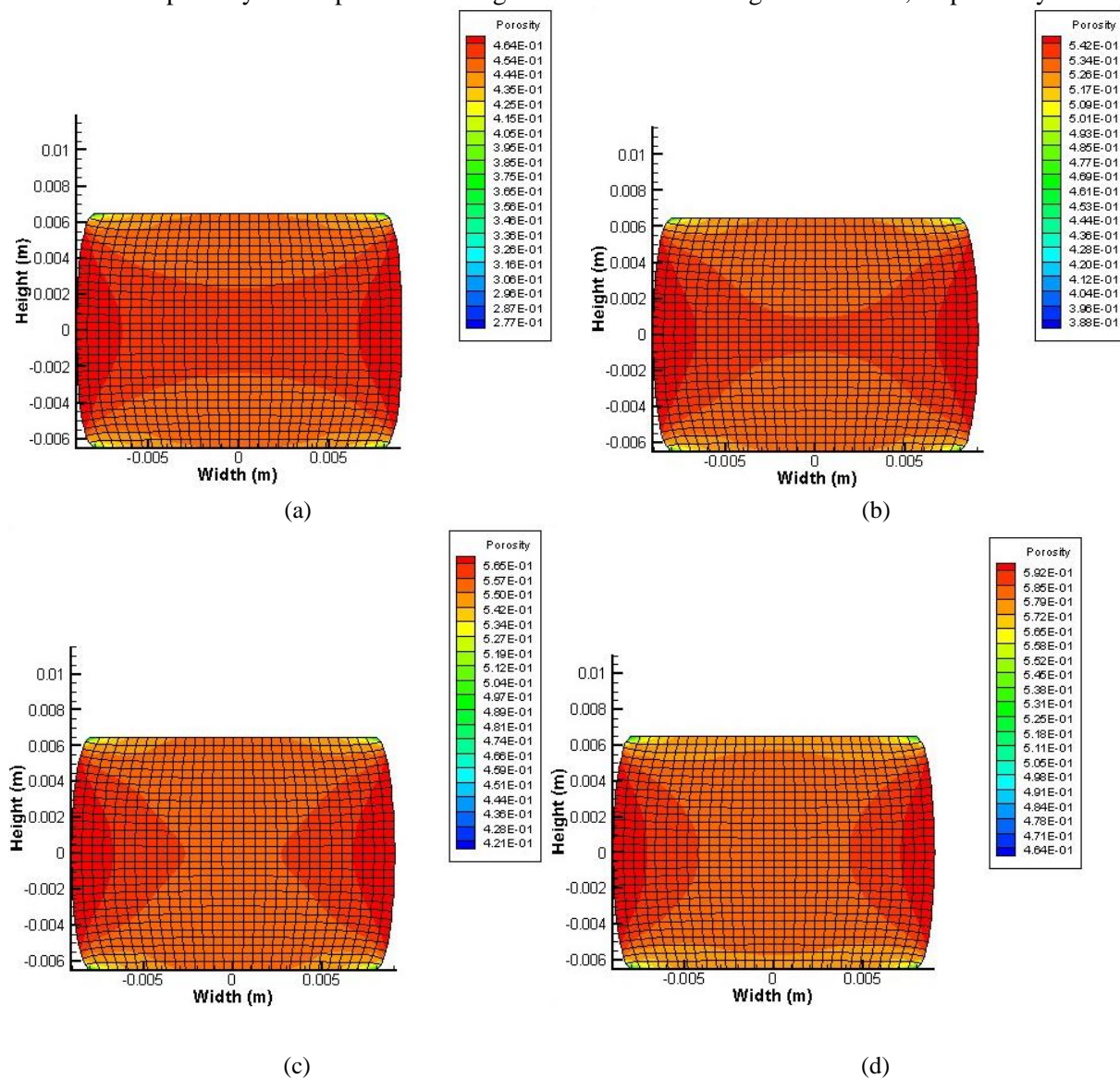
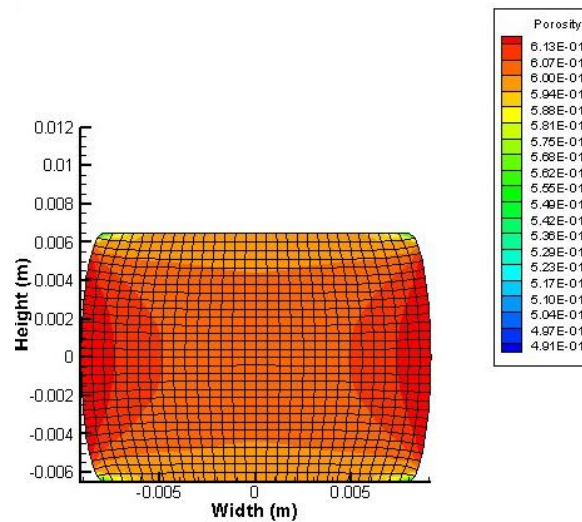


Fig. 9. Contour of porosity of: (a) Sample 2, (b) Sample 3, (c) Sample 4, (d) Sample 5, and (e) Sample 6.

Figure 9 continued.



(e)

6. Conclusion

In this paper, porous Titanium was investigated as a useful material in biomedical usages like human skeleton. It was considered here that in the FEM simulations of porous Titanium, the porosity can be considered as an internal variable in the yield function. To achieve well fitness to experimental data, adjusting parameters which simulate the effects of physical sources on the stress-strain curves of porous Titanium were considered as the coefficients of modified Gurson model which were different from what reported by Tvergaard and Needleman. Results showed that choosing of $q_1 = 1.45$ for porous Titanium with initial porosity of 50.6 % and $q_1 = 1.38$ for other samples with porosity up to 63.9% can completely fit the numerical results to experimental data.

It was shown that the increase of yield stress in stress-strain curves was resulted from both matrix hardening and evolution of porosity during compaction. This result showed constant value of porosity cannot be real assumption due to evolution of porosity. This was proved by the fact that during compression test the porous materials are more aggregated. It was shown that the volume constancy is not satisfied due to the role of trace of stress tensor in the yield criterion and also, evolution of porosity. Moreover, the presence of porosity changed stress distribution and this may affect the shear banding.

7. References

1. L.J. Gibson, Biomechanics of cellular solids, *Journal of biomechanics*, 38 (2005) 377–99.
2. G. Ryan, A. Pandit and D.P. Apatsidis, Fabrication methods of porous metals for use in orthopaedic applications, *Biomaterials*, 27 (2006) 651–70.
3. S.R. Nagaraja, S.G. Rakesh, J.K. Prasad, P.K. Barhai and G. Jagadeesh, Investigations on micro-blast wave assisted metal foil forming for biomedical applications, *International Journal of Mechanical Sciences*, 61 (2012) 1–7.
4. A. Merdji, B. Bachir Bouiadjra, T. Achour, B. Serier, B. Ould Chikh and Z.O. Feng, Stress analysis in dental prosthesis, *Computational Materials Science*, 49 (2010) 126–133.
5. J.D. Bobyn, R.M. Pilliar, H.U. Cameron and G.C. Weatherly, The optimum pore size for the fixation of porous-surfaced metal implants by the ingrowth of bone, *Clinical Orthopaedics & Related Research*, 150 (1980) 263–270.

6. H. Cameron, Six-year results with a microporous-coated metal hip prosthesis, *Clinical Orthopaedics & Related Research*, 208 (1986) 81–83.
7. J. Bobyn, E. Mortimer, A. Glassman, C. Engh, J. Miller and C. Brooks, Producing and avoiding stress shielding: laboratory and clinical observations of noncemented total hip arthroplasty. *Clinical Orthopaedics & Related Research*, 274 (1992) 79–96.
8. M. Schneider and H. Yuan, Experimental and computational investigation of cyclic mechanical behavior of sintered iron, *Computational Materials Science*, 57 (2012) 48–58.
9. J. Kovacic, Correlation between Young's modulus and porosity in porous materials, *Journal of Materials Science Letters*, 18 (1999) 1007–1010.
10. J. Tirosh and D. Iddan, Forming analysis of porous materials, *International Journal of Mechanical Sciences*, 31 (1990) 949–965.
11. H. Nakajima, Fabrication, properties and application of porous metals with directional pores, *Progress in Materials Science*, 52 (2007) 1091–1173.
12. L.J. Gibson and M.F. Ashby, *CellularSolid: Structure and properties*, Cambridge University Press (1988).
13. T. Imwinkelried, R. Biomaterials, S. Gmbh and C. Oberdorf, Mechanical properties of open-pore Titanium foam, *Journal of Biomedical Materials Research Part A* (2007).
14. R. Singh, P.D. Lee, T.C. Lindley, C. Kohlhauser, C. Hellmich, M. Bram, T. Imwinkelried and R.J. Dashwood, Characterization of the deformation behavior of intermediate porosity interconnected Ti foams using micro-computed tomography and direct finite element modeling, *Acta biomaterialia*, 6 (2010) 2342–51.
15. W. Niu, S. Gill, H. Dong and C. Bai, A two-scale model for predicting elastic properties of porous Titanium formed with space-holders, *Computational Materials Science*, 50 (2010) 172–178.
16. M.R. Karamooz Ravari, M. Kadkhodaei, M. Badrossamay and R. Rezaei, Numerical investigation on mechanical properties of cellular lattice structures fabricated by fused deposition modeling, *International Journal of Mechanical Sciences*, 88 (2014) 154–161.
17. C.C. Huang and J.H. Cheng, Forging simulation of sintered powder compacts under various frictional conditions, *International Journal of Mechanical Sciences*, 44 (2002) 489–507.
18. S.B. Biner and W.A. Spitzig, Densification of iron compacts with various initial porosities under hydrostatic pressure, *Acta Metallurgica*, 38 (1990) 603–610.
19. V. Tvergaard, Influence of voids on shear band instabilities under plane strain conditions, *International Journal of Fracture*, 17 (1981) 389–407.
20. V. Tvergaard and A. Needleman, Analysis of the cup-cone fracture in a round tensile bar, *Acta Metallurgica*, 32 (1984) 157–169.
21. R. Becker, A. Needleman, O. Richmond and V. Tvergaard, Void growth and failure in notched bars, *Journal of the Mechanics and Physics of Solids*, 36 (1988) 317–351.
22. M. Abbasi, M. Ketabchi, H. Izadkhah, D.H. Fatmehsaria and A.N. Aghbash, Identification of GTN model parameters by application of response surface methodology, *Procedia Engineering*, 10 (2011) 415–420.
23. W.A. Spitzig, R.E. Smelser and O. Richmond, The evolution of damage and fracture in iron compacts with various initial porosities, *Acta Metallurgica*, 36 (1988) 1201–1211.
24. J. Simo and T. Hughes, *Computational Inelasticity*, Springer, New York, (2013).
25. T. Belytschko, K. Wing and B. Moran, *Nonlinear Finite Elements For Continua And Structures*, John Wiley & Sons, (2014).

شبیه‌سازی رفتار تغییر شکل تیتانیوم متخلخل با استفاده از تابع تسلیم گارسون اصلاح شده

احسان انصاری بصیر، کیوان نارویی

دانشکده مهندسی و علم مواد، دانشگاه صنعتی خواجه نصیرالدین طوسی، تهران، ایران.

چکیده: در این مقاله منحنی تنش- کرنش تیتانیوم متخلخل به عنوان یک ماده مورد استفاده در پزشکی با استفاده از خواص مکانیکی تیتانیوم متراکم پیش‌بینی شد. از معیار اصلاح شده گارسون برای پیش‌بینی رفتار پلاستیک تیتانیوم متخلخل در فرایند فشرده سازی استفاده شد. مقادیر مختلف پارامترهای معیار گارسون اصلاح شده برای مقادیر متفاوت تخلخل اولیه استفاده شد. مشاهده شد فرض حجم ثابت در حین تغییر شکل پلاستیک در محیط متخلخل به علت وجود تخلخل و سهم تنش هیدروستاتیکی در معیار تسلیم نمی‌تواند برآورده شود. مشاهده شد محاسبه تغییرات تخلخل در حین تغییر شکل برای مدل‌سازی دقیق مورد نیاز می‌باشد. همچنین انبساط جانبی نمونه‌های متخلخل نسبت به نمونه متراکم در یک جابه‌جایی محوری یکسان بیشتر بود. توزیع تنش در نمونه‌های متخلخل متفاوت با نمونه‌های متراکم بود که این مساله سبب پیش‌بینی متفاوت باندهای برشی می‌گردد. ارزیابی تغییرات کسر تخلخل در حین تغییر شکل منجر به رفتار شبه خطی در منطقه تغییر شکل پلاستیک گردید.

کلمات کلیدی: مدل گارسون اصلاح شده، تیتانیوم متخلخل، اجزا محدود، تغییر شکل پلاستیک، فشرده سازی.